Contents lists available at ScienceDirect

Journal of Magnetism and Magnetic Materials

journal homepage: www.elsevier.com

Research articles

Effect of Cu-electrodeposition on the magnetic properties of Sr-hexaferrite with porous structure

F.J. Santos-López[a], D.L. Espericueta[b], I.E. Castaneda-Robles[c], M. Mirabal-García[d], S. Aranda-Espinoza[d], J.M. Martínez-Huerta[e], A. Lobo Guerrero[a,*]

[a] Área Académica de Ciencias de la Tierra y Materiales, Universidad Autónoma del Estado de Hidalgo, Carretera Pachuca Tulancingo km 4.5, Ciudad del Conocimiento, Mineral de la Reforma, Hgo., Mexico
[b] Instituto Tecnológico Superior de San Luís Potosí, Carr. 57 México-Piedras Negras km. 189, S.L.P., Mexico
[c] Área Académica de Ingeniería y Arquitectura, Universidad Autónoma del Estado de Hidalgo, Carretera Pachuca Tulancingo km 4.5, Ciudad del Conocimiento, Mineral de la Reforma, Hgo., Mexico
[d] Instituto de Física, Universidad Autónoma de San Luis Potosí, Manuel Nava 6, Zona Universitaria, 78290 San Luis Potosí, S.L.P., Mexico
[e] Instituto Potosino de Investigación Científica y Tecnológica, Camino a la presa de San José sn. Lomas cuarta sección, San Luis Potosí, S.L.P., Mexico

ARTICLE INFO

Keywords:
Magnetic ceramic
Electrochemical deposition
Magnetic coupling
Foam hexaferrite
Switching field distribution

ABSTRACT

The magnetic behavior of the strontium hexaferrite (SrM) with foam structure was studied when copper (Cu) coats its surface. Copper was successfully deposited on the walls of the magnetic foam using the electrodeposition method. Results suggest that copper begins to nucleate on the hexaferrite grains because of a two steps process; the one based on a driving force of the Cu ions by the effect of the electric field, and secondly, the deposition of copper atoms on the non-conductive SrM surface. The SrM and Cu show a hard interaction which modifies the magnetic properties of the SrM foam as copper covers its surface. Hence, the coercive field (H_c) and the magnetization squareness (M_r/M_s) have a trend to increase up to a Cu/SrM weight ratio close to 0.5. The dM/dH, M curves (SFD) indicate the presence of two uncoupled magnetic contributions. The copper fixes the magnetic moments of iron at the surface increasing the switching field these particles, whereas in the inner particles the magnetization rotates easily resulting in a widening of the SFD curve.

1. Introduction

Over the past few years, the electrochemical method has been identified as a good option to produce multifunctional materials. Several pure metals, binary and ternary alloys, and nanostructured metallic materials have been reported using electrochemistry techniques [1–5]. The ability of this method to control the growth conditions, including composition, crystallographic structure, texture, and grain size, gives the possibility to study new functional properties, as well as the coupling interactions and other phenomena that are present at the interface between the different components [6–8]. The electrodeposition method is based on the reduction of metal ions contained in a solution to form a metallic film over a generally metallic substrate [9]. Nevertheless, there exist a series of variations for the method in which it is possible to induce a film growth on non-conductive substrates with the use of additives as a catalyst [10]. It has been also reported a successful metallic film growth in a poorly conductive matrix using an overpotential [11,12]. Even though metals are easiest to obtain, some semiconductor materials and non-metallic elements can be co-deposited by using electrodeposition [9].

Copper is one of the most thoroughly studied electrodeposited materials, and it is widely used in electronic applications because of its conductivity properties. Besides, in the past few years, electrodeposited soft-magnetic materials based on nickel, iron, and cobalt have also been intensively studied finding practical application as inductive components and magnetic field sensors, while electrodeposition of hard-magnetic materials is being developed [9].

The strontium hexaferrite is a hard-magnetic ceramic material widely used because of its high chemical stability and low manufacturing costs. Usually, the straightforward application of these type of magnetic ceramics is as solid pieces. However, the use of porous-reticulated structures may present some advantages such as high superficial area, low weight and low thermal conductivity [13,14]. Previous works report the obtention of M-type hexaferrite with porous-reticulated structure [15]. These first studies have shown the feasibility to fabricate

* Corresponding author.
Email address: azdlobo@gmail.com (A. Lobo Guerrero)

https://doi.org/10.1016/j.jmmm.2019.02.039
Received 17 September 2018; Received in revised form 13 February 2019; Accepted 14 February 2019
Available online xxx
0304-8853/

magnetic porous ceramics in a simple form. Also, they opened up the possibility to develop advanced magnetic composite materials using these structures as a skeleton.

The magnetostatic interactions in porous structures play an important role in the determination of the magnetic state. These interactions are closely dependent on the porous characteristics, and they have a demagnetizing effect [16,17]. One main characteristic in porous-reticulated structures is their large superficial area. Also, it is well known that the interaction between a magnetic material with a metallic and non-magnetic film can alter the magnetic behavior [18]. The effect of copper electrodeposition on the surface of magnetic SrM with porous-reticulated structure has been for the first time studied in this work. Also, we detail the methodology to deposited metallic atoms on a ceramic-non-conductive surface using a modification of the well-known chemical electrodeposition method. The success in obtaining one magnetic ceramic structure covered with one thin metallic layer opens the possibility to study phenomena occurring at surface level and to develop multifunctional materials required in modern technologies.

2. Experimental

Magnetic ceramics with porous structures were fabricated using a combination of the ceramic and the replication methods. Iron oxide (Fe_2O_3 Sigma-Aldrich, 99%) and strontium carbonate ($SrCO_3$ Sigma-Aldrich, 99.9%) were weighed in a stoichiometric ratio, and then powders were mixed with ethylic alcohol for 2 h at 90 rpm using a planetary mill Fritsch Pulverisette 5 to homogenize the mixture. Afterward, the powders were dried at 60 °C. Once dried, the powders were mixed in a ratio 1:1 with Arabic gum (Sigma-Aldrich) which acts as binder and avoids the structure collapses during the heat-treatment. The powder with the binder was mixed in the agate mortar for 10 min. Then, another part in weight of ethylene glycol (C_2HO_2 Fluka, 99.5%) was added as a liquid phase; all the components were newly mixed for 10 min to obtain a slurry of hexaferrite precursors. The polyurethane sponges used as pattern were compressed and immersed in the slurry of precursors. Then, they decompress inside of the sludge so that the foam absorbs the mixture of precursors. The sponges impregnated with the slurry were heat-treated using a Carbolite RHF 15/3 furnace. First, using a slope of 1 °C/min up to 600 °C, then, temperature increases at 2 °C/min up to 1380 °C, maintaining this temperature for two hours and hence, the samples were left to cool down inside of the furnace up to room temperature. A detailed procedure to fabricate ceramic foams can be consulted in Ref. [17].

The electrodeposition of copper on the surface of foam hexaferrite was done with a homemade electrochemical system and using a commercial electrolyte bought from CASWELL. A copper plate was used as an anode, and the ceramic foam was connected through the hexaferrite pores using a copper wire without varnish which also acts as a cathode. Finally, a 4.5 DC voltage was fixed between electrodes using a laboratory power supply EA-PS 2032-025.

The resulting samples were characterized by using optical microscopy for several electrodeposition times using a digital microscope. The crystalline parameters, phase purity and quantitative phase analysis were obtained from X-ray diffraction (DRX) with a Siemens D5000 diffractometer with a cobalt source ($\lambda = 1.7890$ Å) and using the Rietveld method incorporated in the MAUD program [19]. Gravimetric analysis was done varying the electrodeposition time using an analytical precision balance enabled to resolve up to 0.1 mg. The morphology and microstructural characteristics were observed using an Inspect F50 scanning electron microscope (SEM) operated at 30 kV. The magnetic properties were analyzed from the hysteresis loops at different Cu contents. The SFD curves were obtained from the direct derivative of the demagnetizing branch of the hysteresis loops. The magnetic measurements were performed at room temperature using an alternating gradient magnetometer (AGM) of Princeton Micromag 2900.

3. Results and discussion

Fig. 1 shows optical micrographs of the strontium hexaferrite foams after they were subject to copper electrodeposition at various immersion times, and a reference sample without electrolytic treatment. Reference sample shows a characteristic gray hue and empty cavities are abundant at each wall due to the CO_2 flow produced as the polyurethane pattern burns during heat-treatment. The sample with an immersion time of 3 min in the electrolytic bath shows a brilliant film surrounding all the walls of the porous hexaferrite. Then, when immersion time increases, it is observed that the thickness of the metallic film growths. The sample with 20 min immersion shows a thick coating covering all hexaferrite surface.

X-ray diffractograms were obtained in order to investigate the chemical composition of the deposited material on the surface of the hexaferrite foam. Fig. 2(a) shows the X-ray pattern of the hexaferrite foam obtained at a sintering temperature of 1280 °C. The Rietveld analysis indicates only the presence of the M-type structure (hexagonal $P6_3/mmc$). The structural parameters are shown in Table 1. Whereas Fig. 2(b) shows the X-ray pattern of the strontium hexaferrite foam subject to the electrodeposition treatment for 7 min. In this case, the Rietveld analysis indicates the presence of both copper (cubic Fm-3m) observed on the surface and the strontium hexaferrite at the core. According to the phase analysis, this sample presents 41.5 %wt of copper and 58.5 %wt of the SrM. No other phases could be detected by X-ray diffraction. Although eventual oxidation of the Cu-surface is expected, the inner deposits would remain unchanged. Low counts and texture effects observed in X-ray patterns result from the diffraction of the reticulated structures.

The copper mass increment is presented in Fig. 3 as a weight's ratio Cu/SrM in function of time. The gravimetric analysis was performed after hexaferrite foams were electrodeposited, then the foams were washed with ethyl alcohol and dried at room temperature. Under these conditions, it was observed three regions associated with different deposition mechanisms. The first stage corresponds from zero to 3 min with Cu presence reaching ~10% of total weight. In this case, copper was electrodeposited over a non-conductive ceramic following a linear trend with a slope of 0.033, as the insert of the Fig. 3 shows. The second stage ranges from 3 min up to 20 min, that is, above 10 %wt, and up to ~150 %wt. Here, the velocity of deposition increases with a slope of 0.085. The final stage occurs parallel to the 20–60 min treatment period and corresponds to a Cu content higher than 150 %wt. In this case, the deposition rate decays, and the obtained curve slope was of 0.006. As stated above, the behavior observed in the gravimetric measurements has been related with three different deposition mechanisms. The early stage involves the copper nucleation over the SrM surface. If we consider the poor-conductive properties of the hexaferrite compounds, then, an electrostatic process assists the copper nucleation on the SrM surface. Although transport properties have been little-studied in hexaferrite compounds, experimental evidence points to surface polarization and small polaron hopping as the main conduction mechanisms which hexaferrite compounds can exhibit [20,21]. The first deposited Cu atoms create a concentration gradient which accelerates the copper flux to the cathode, these first atoms cluster in small groups, to later grow and join to the adjacent clusters, giving place to a uniform coating. Detailed observations suggest that this nucleation occurs in the whole surface and not only at regions close to the cathode contact. Once Cu nucleates over all the SrM surface, new copper starts to grow over early copper, at this point, the deposition rate increases because of the copper conductive properties. Finally, the rapid copper-coat growth slows down drastically. In this sense, each one of the as-mentioned

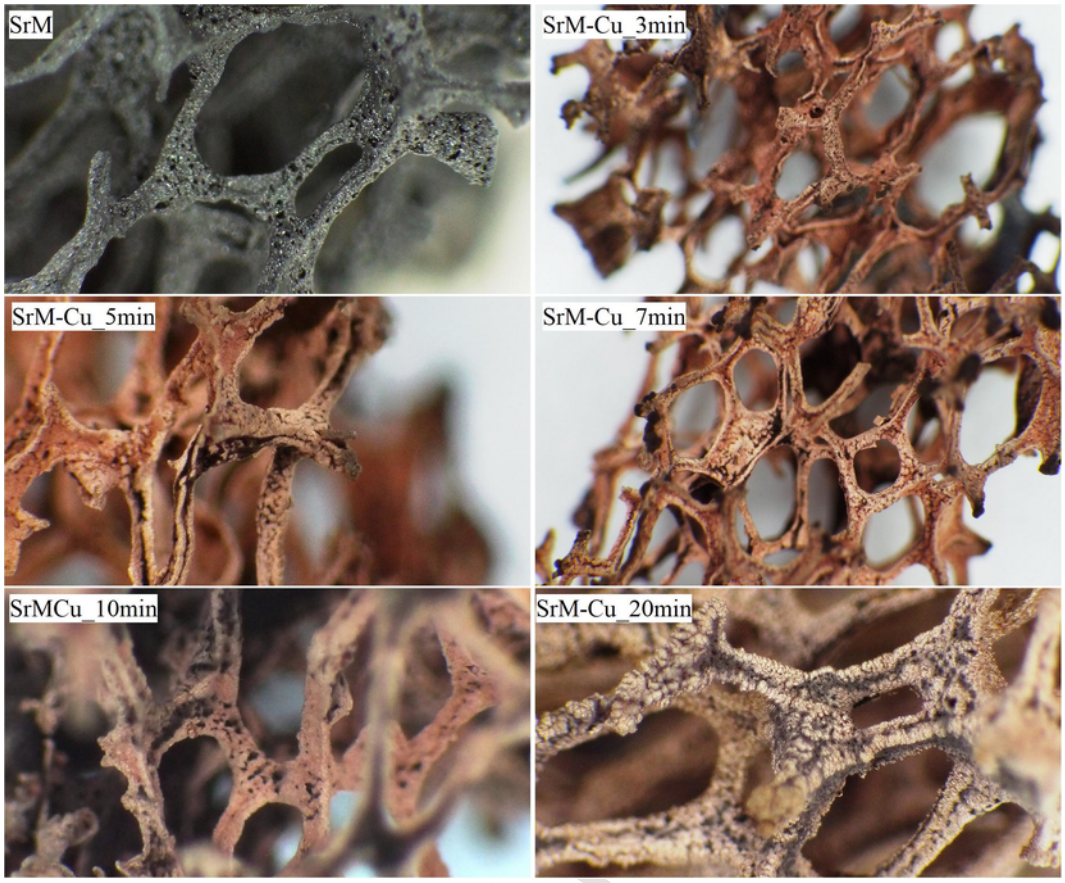

Fig. 1. Optical micrographs of the strontium hexaferrite (SrM) at different stages of the copper electrodeposition.

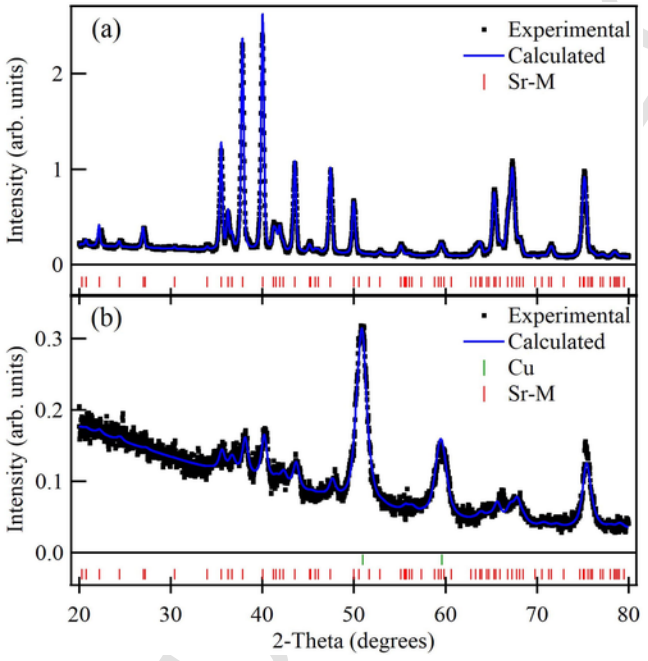

Fig. 2. X-ray diffractograms and the Rietveld fit of (a) SrM pure phase with foam structure, and (b) SrM foam with the Copper cover.

stages needs to be carefully studied both theoretically and experimentally to completely understand the deposition mechanism.

An irregular foam surface composed of grains with hexagonal plate-shape and broad size distribution is observed in the SEM micrographs of Fig. 4. This particle configuration with large grains together small ones helps to improve the mechanical properties of the foam structure avoiding their collapse during the heat-treatment or during its subsequent handling. Also, the surface presents pores distributed along the walls and inside of them, indicating that this structure has internal empty cavities and is not completely filled with hexaferrite particles.

Fig. 5 shows the SEM micrographs of the SrM foam with the copper cover varying the electrodeposition time from 3 to 20 min. Dark-gray is associated with the SrM phase, while light-gray corresponds to deposited copper. When the hexaferrite is immersed in the electrolytic bath for 3 min at a constant potential of 4.5 V, it is observed a copper deposition covering grains and filling the pores located at surface level. This indicates that Cu nucleates independently of the wire contact position, which is an exciting result because the hexaferrite is a non-conductive material. Once nucleated, copper organizes in clusters to form a popcorn morphology. Also, in this micrograph it has been highlighted internal cavities located in a transverse rupture, which proves that the internal skeleton of the hexaferrite phase is partially empty because of the polyurethane pattern disintegration, followed by grains growth during the heat-treatment. The sample of 5 min shows a copper cover wherein new deposited material exhibits a stalagmite type growth and formation of bubbles as a consequence of hydrogen (H^+) production during the electrodeposition process. After 7 min, the deposited copper forms particles with droplet morphology resulting from nucleation of new clusters on the inner copper. At this point, the Cu deposits reach 45 μm above of the hexaferrite surface. A frost morphology was formed in the sample with 20 min; this may be related with the inhibition of the copper grow shown in Fig. 5. Furthermore, the sample size became a critical parameter which changes the morphology and on the thickness of the copper layer, because on smaller samples copper deposited

Table 1
Structural parameters and phase analysis obtained from the Rietveld refinement method.

Sample ID	Detected Phases	wt (%)	Symmetry	Spatial group	Cell parameters (Å)	Crystallite size (nm)	X-ray density (g/cm^3)
SrM	SrM	100	Hexagonal	$P6_3/mmc$	a = 5.8685 (2) c = 23.0059 (7)	83 (1)	5.138
SrM-Cu_7min	SrM	58.5	Hexagonal	$P6_3/mmc$	a = 5.8685 (2) c = 23.0059 (7)	83 (1)	5.138
	Cu	41.5	Cubic	Fm-3m	a = 3.6089 (3)	14 (1)	8.979

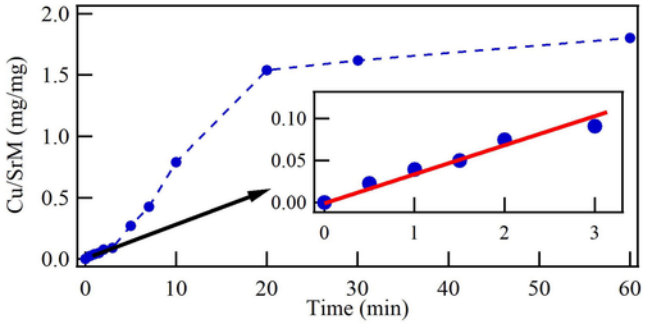

Fig. 3. Rate of copper deposition from zero to 60 min. The inset shows the deposition rate from zero to 3 min.

faster than in the bigger ones. Then, the following results are presented normalized with respect to the SrM mass for each sample. A significant result is that copper can be deposited over all the SrM surface, which is a non-conductive ceramic, and without the use of any additive or catalyst, this opens the possibility to create conductive patterns fixed in a magnetic ceramic.

Fig. 6 shows the hysteresis loops of the SrM with copper at different electrodeposition times, and as a reference, we included the magnetization curve of the SrM measured as powder and as foam without copper. The powder presents a coercive field (H_c) of 2.5 kOe with a remanence squareness (M_r/M_s) of 0.5 and magnetization saturation (M_s) of 73 emu/g, which are typical values for this compound when it is prepared using the ceramic route. Therefore, when strontium hexaferrite is obtained with the porous structure, the magnetization parameters decrease as result of an increase of the magnetostatic interactions [17]. In the case of the SrM as foam, it has $H_c = 1.0$ kOe, $M_r/M_s = 0.4$ and $M_s = 70$ emu/g. However, when copper is deposited on the SrM foam, it is observed a variation of the magnetization parameters which are dependent on the electrodeposited copper. Fig. 7 shows the variation of the coercive field and the remanence squareness as a function of the Cu/SrM (mg/mg) ratio. There is obtained up to 35% increment in H_c and 52.5% more of the M_r/M_s in the samples with a weight ratio Cu/SrM below of 1/2 (~7 min), taking as reference the uncoated SrM foam. At higher Cu content, the H_c and the M_r/M_s stop to increase and start to decrease. Thus, when the weight ratio of Cu/SrM is around 2/1, the H_c is just 1% above of the one obtained for the SrM foam, whereas the M_r/M_s is 7.5% below. In Table 2 are presented the magnetization parameters of the SrM with electrodeposited Cu, as well as the reference samples. If we take in mind that hexaferrite skeletons are equivalents because they are fabricated using the same template, then the magnetostatic interactions do not have a determinant role in the variation of the magnetization. Accordingly, the initial increase of the magnetization parameters can be attributable to an exchange coupling between copper and iron atoms located near to the hexaferrite surface.

Fig. 8 shows the dM/dH vs. H curves, also called switching field distribution (SFD), which were obtained to study the rotation of the magnetization when Cu is deposited on the hexaferrite surface. The SFD curve is an indicative showing the behavior of the coercive fields when magnetization of the particles rotates as the field is swept from positive saturation to negative saturation, and the wide of the curve is sensitive to the magnetostatic interactions strength [22]. In the reference, SrM powder it is observed one single peak centered at 2.58 kOe with a full-width half-maximum (FWHM) of 2.23 kOe. Now, when SrM is fabricated with a porous structure, the maximum of this curve relocates to a lower field, centered it at 0.96 kOe and the FWHM enlarges up to 2.72 kOe. This behavior is attributable to an increase of the magnetostatic interactions occurred in the porous structure [23,24]. Notwithstanding, when Cu atoms interact with the SrM, the behavior of a single curve is lost and there appear two contributions in the SFD curves. In Fig. 8 the continuous color lines are the fitted contributions to the SFD profiles and the dashed green line is the sum of that contributions. There is one contribution located around 2.0 kOe, labeled as C1 (red line), and other-centered around 0.5 kOe, labeled as C2 (blue line). The C1 is related with the SrM outer layers wherein copper help to fix the magnetization moments of iron and results in a switching field located at bigger fields, with a trend to shift to above fields as Cu goes covering the SrM surface. The contribution C2 is near to zero fields and results from the inner domains away from the surface layers. This contribution prefers to move to a lower field when Cu content increases, maybe because this region could be subject to a big demagnetizing field. The final shape of the SFD curve is controlled by these two un-

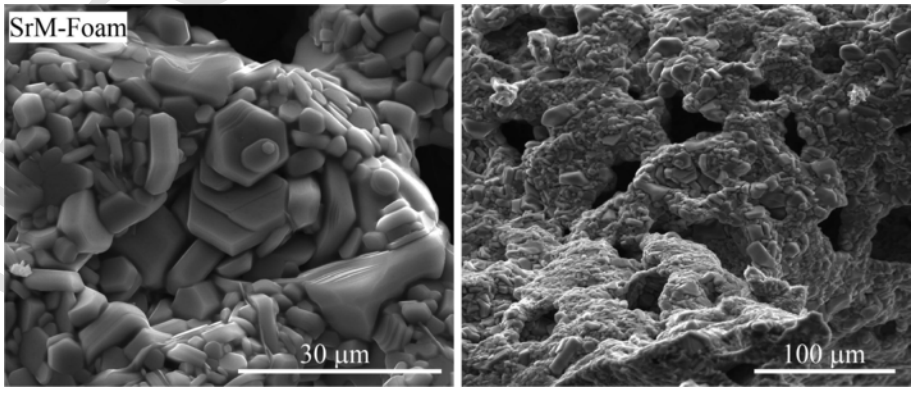

Fig. 4. SEM micrographs of the strontium hexaferrite with a porous structure.

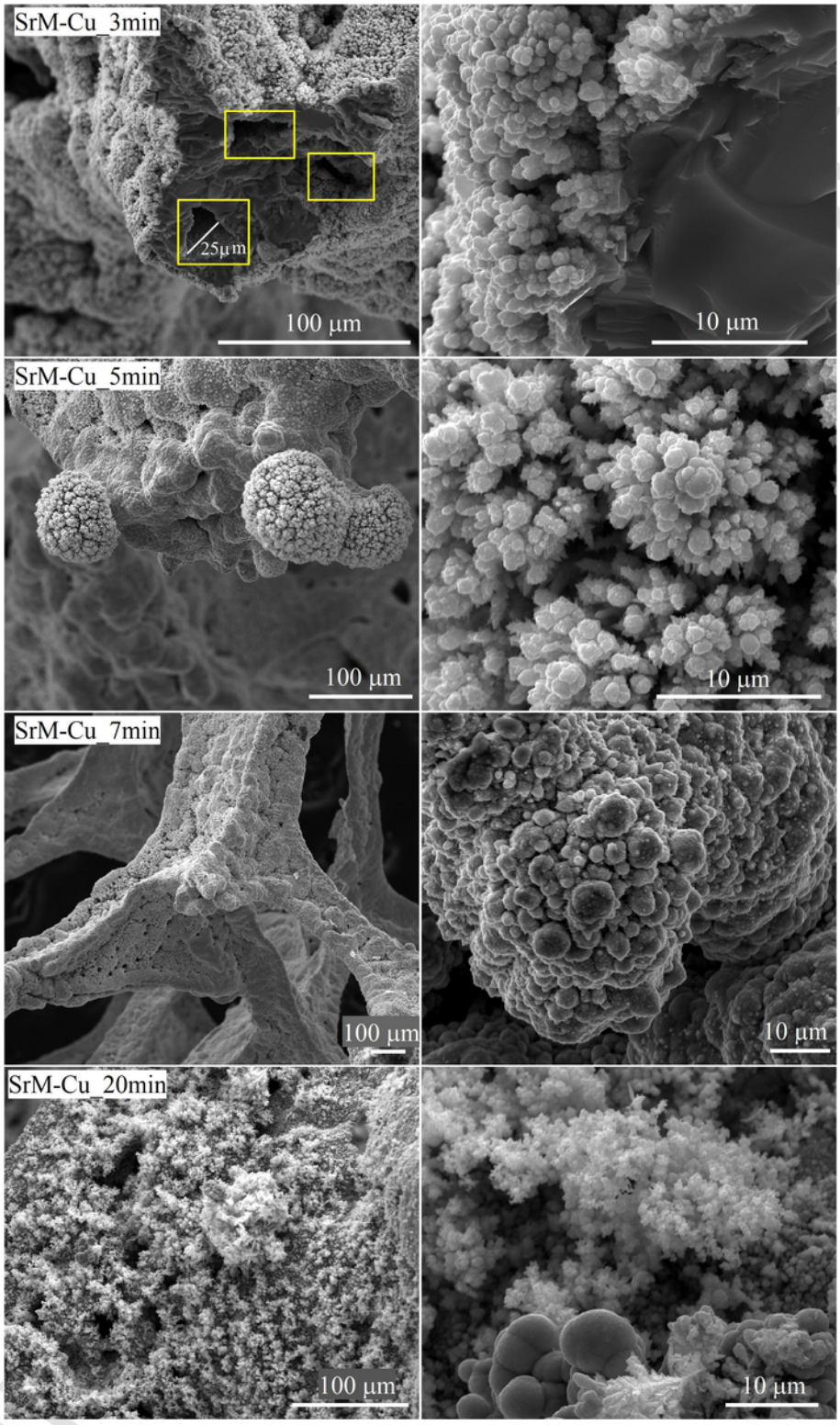

Fig. 5. SEM micrographs at two different magnifications of the SrM, as a porous structure with electrodeposited copper at various immersion times.

coupled contributions, acting independently each of the other, in the same way, the coercive field is determined by the way in which these two contributions balanced. Then, the interaction between Fe-Cu occurs at surface level and in this case, both contributions (surface and inner) are comparable because of the large surface area having the porous hexaferrite.

The results discussed above show, firstly that the deposition of a metallic layer over hexaferrite ceramic surface is possible. Although additional studies are required to gain more understanding of the electrodeposition mechanism on the hexaferrite surface, this feature opens the possibility to developed hexaferrite based composites using other metallic shells, such as nickel or cobalt, allowing to study the coupling

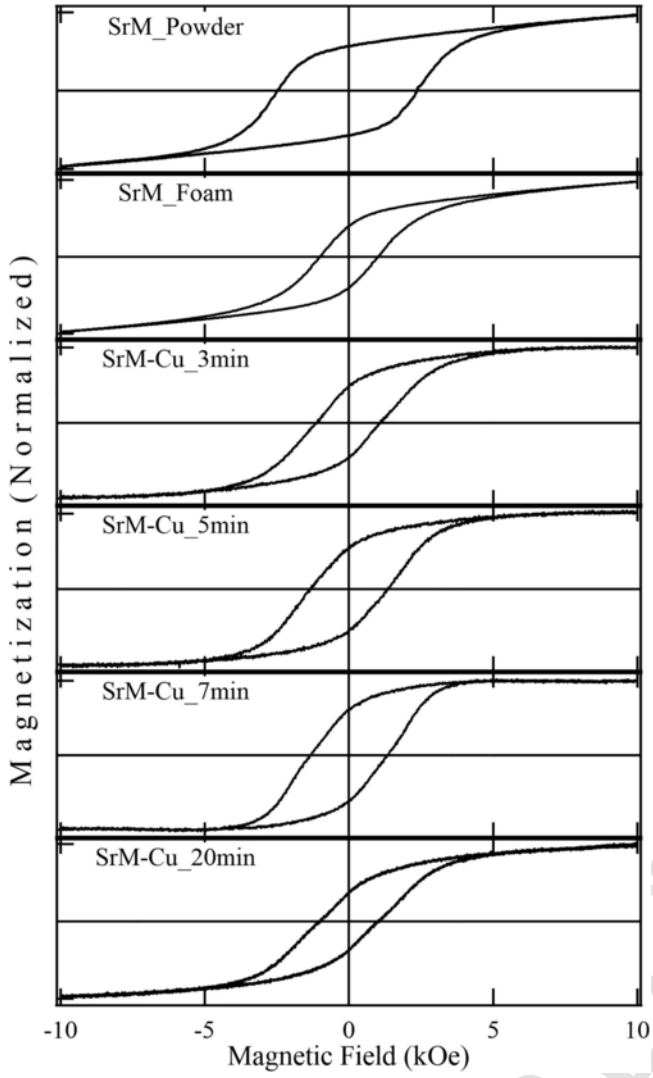

Fig. 6. Normalized hysteresis loops of the SrM as powder, foam, and foams covered with Cu at various electrodeposition times.

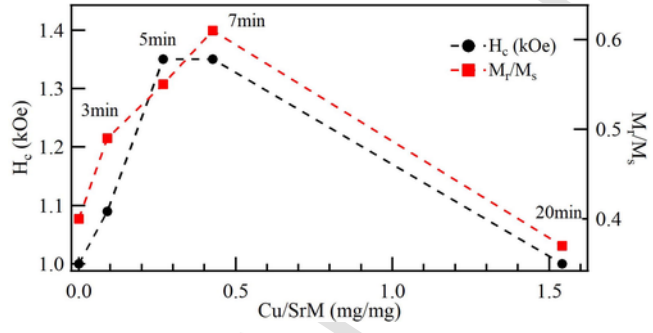

Fig. 7. Magnetic behavior of the SrM with foam structure at various Cu/SrM weight ratios.

between soft and hard magnetic materials. Secondly, resulting from the physical interaction strongly linked to the copper thickness, there is workable to take advantage of effects originated at the interface. One possibility is designing copper patterns on the hexaferrite surface, and overlapping an induced field with the hexaferrite magnetization. This could be an outcome in a tunable net magnetization. Another promising application would be in electromagnetic interference shielding because of its light weight, resistance to corrosion and the combined electrical properties of copper and the microwave absorbing ability of the hexaferrite.

Table 2
Magnetization properties of SrM foams with copper and the reference samples.

Sample	Cu/SrM (mg/mg)	H_c (kOe)	Mr/Ms	SFD_C (kOe)	SFD_{FWHM} (kOe)
SrM-Powder	–	2.50	0.50	2.66	2.23
SrM-Foam	–	1.00	0.40	1.00	2.72
SrM-Cu_3m	0.0909	1.09	0.49	1.31	3.24
SrM-Cu_5m	0.2687	1.35	0.55	1.41	3.09
SrM-Cu_7m	0.4268	1.35	0.61	1.44	2.87
SrM-Cu_20m	1.5415	1.01	0.37	1.25	3.72

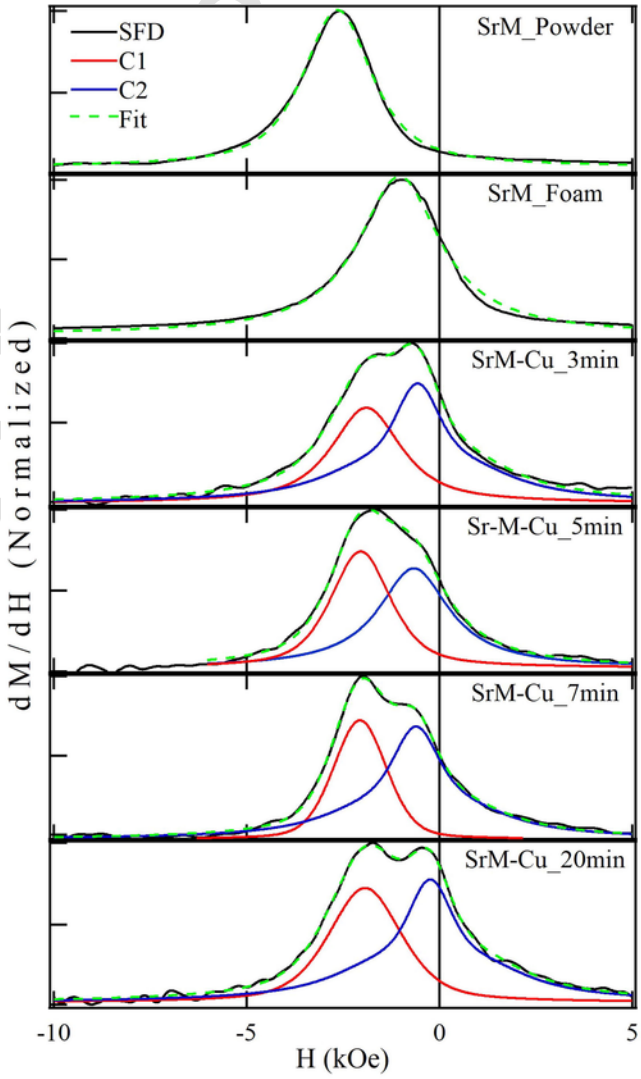

Fig. 8. Normalized d*M*/d*H*, *M* curves of the SrM as powder, foam, and the foams with Cu, showing two uncoupled magnetic contributions for the samples with copper.

4. Conclusion

The copper deposition on the surface of the strontium hexaferrite with foam structure shown a change on the SrM magnetic properties.

This variation is attributable to a strong interaction occurred between copper atoms and the iron of the SrM, which fixes their magnetic moments making difficult their alignment with respect to an external field. However, there is a competition between the surface effects with the highly demagnetizing property of the deeper SrM grains, wherein at high Cu contents, the surface magnetizing effects are obscured.

Acknowledgments

Authors thank G.G. López Rocha (IF-UASLP) for his lab assistants and Carolina Medina (UC-Davis) for her critical reading.

Appendix A. Supplementary data

Supplementary data to this article can be found online at https://doi.org/10.1016/j.jmmm.2019.02.039.

References

[1] B.P. Relekar, S.A. Mahadik, S.T. Jadhav, A.S. Patil, R.R. Koli, G.M. Lohar, V.J. Fulari, Effect of electrodeposition potential on surface free energy and supercapacitance of MnO_2 thin films, J. Electron. Mater. 47 (2018) 2731.

[2] G. Yar-Mukhamedova, M. Ved, N. Sakhnenko, T. Nenastina, Electrodeposition and properties of binary and ternary cobalt alloys with molybdenum and tungsten, Appl. Surf. Sci. 445 (2018) 298.

[3] J.C. García-Mayorga, G. Urbano-Reyes, M.A. Veloz-Rodríguez, V.E. Reyes-Cruz, J.A. Cobos-Murcia, J. Hernández-Ávila, M. Pérez-Labra, Electrochemical preparation of precursor phases for obtaining alpha-alumina from aluminium scrap, Ceram. Int. 44 (2018) 7435.

[4] C.-Y. Huang, C.-J. Hsiao, C.-C. Lin, C.-S. Lin, J.-Y. (James) Chang, C.-K. Sung, S.-C. Wang, T.-S. Chin, A novel CoCuP electrodeposited film with improved planar hard magnetic properties and film quality, Surf. Coat. Technol. 350 (2018) 890.

[5] J. Li, G. Zhou, X. Jin, Y. Hong, W. He, S. Wang, Y. Chen, W. Yanga, X. Su, Direct activation of copper electroplating on conductive composite of polythiophene surface-coated with nickel nanoparticles, Comp. Part B: Eng. 154 (2018) 257.

[6] M. Darques, L. Piraux, A. Encinas, P. Bayle-Guillemaud, A. Popa, U. Ebels, Electrochemical control and selection of the structural and magnetic properties of cobalt nanowires, Appl. Phys. Lett. 86 (2005) 072508.

[7] C.E. Carreón-González, J. De La Torre Medina, L. Piraux, A. Encinas, Electrodeposition growth of nanowire arrays with height gradient profiles for microwave device applications, Nano Lett. 11 (2011) 2023–2027.

[8] F. Niknia, F. Jamali-Sheini, R. Yousefi, M. Cheraghizade, Effect of thickness on the optoelectronic properties of electrodeposited nanostructured SnS films, Opt. Quantum Electron. 50 (2018) 339.

[9] W. Ruythooren, K. Attenborough, S. Beerten, P. Merken, J. Fransaer, E. Beyne, C. Van Hoof, J. De Boeck, J.P. Celis, Electrodeposition for the synthesis of microsystems, J. Micromech. Microeng. 10 (2000) 101.

[10] S. Ono, K. Naitoh, T. Osaka, Initial propagation stage of direct copper plating on non-conducting substrates, Electrochim. Acta 44 (1999) 3697.

[11] J.M. Ortega, Electrodeposition of copper on poly(o-aminophenol) modified platinum electrode, Thin Solid Films 360 (2000) 159.

[12] G.K. Chandler, D. Pletcher, The electrodeposition of metals onto polypyrrole films from aqueous solution, J. Appl. Electrochem. 16 (1986) 62.

[13] C. Witherspoon, P. Zheng, M. Chmielus, D.C. Dunand, P. Müllner, Effect of porosity on the magneto-mechanical behavior of polycrystalline magnetic shape-memory Ni–Mn–Ga foams, Acta Mater. 92 (2015) 64.

[14] S. Hamidizadeh, A. Ataie, A. Nozari, Synthesis and characterization of porous nano-crystalline barium hexaferrite, Adv. Mater. Res. 622 (2013) 860.

[15] U. Topal, H.I. Bakan, Permanently magnetic $BaFe_{12}O_{19}$ foams: synthesis and characterization, Mater. Chem. Phys. 123 (2010) 121.

[16] U. Topal, H.I. Bakan, Magnetic properties and remanence analysis in permanently magnetic $BaFe_{12}O_{19}$ foams, J. Eur. Ceram. Soc. 30 (2010) 3167.

[17] A.L. Guerrero, D.L. Espericueta, S.A. Palomares-Sánchez, J.T. Elizalde-Galindo, B.E. Watts, M. Mirabal-García, Preparation and magnetic properties of the Sr-hexaferrite with foam structure, J. Magn. Magn. Mater. 419 (2016) 442.

[18] W. Weber, C.H. Back, A. Bischof, D. Pescia, R. Allenspach, Magnetic switching in cobalt films by adsorption of copper, Nature 374 (1995) 788.

[19] L. Lutterotti, S. Matthies, H.-R. Wenk, A.J. Schultz, J. Richardson, Combined texture and structure analysis of deformed limestone from neutron diffraction spectra, J. Appl. Phys. 81 (1997) 594.

[20] R. Pattanayak, S. Panigrahi, T. Dash, R. Muduli, D. Behera, Electric transport properties study of bulk $BaFe_{12}O_{19}$ by complex impedance spectroscopy, Phys. B 474 (2015) 57.

[21] Rujun Tang, Hao Zhou, Run Zhao, Jie Jian, Han Wang, Jijie Huang, Meng Fan, Wei Zhang, Haiyan Wang, Hao Yang, Dielectric relaxation and polaronic conduction in epitaxial $BaFe_{12}O_{19}$ hexaferrite thin film, J. Phys. D Appl. Phys. 49 (2016) 115305.

[22] M. Ranjbar, A.K.G. Tavakkoli, S.N. Piramanayagam, K.P. Tan, R. Sbiaa, S.K. Wong, T.C. Chong, Magnetostatic interaction effects in switching field distribution of conventional and staggered bit-patterned media, J. Phys. D: Appl. Phys. 44 (2011) 265005.

[23] R. Murillo-Ortíz, M. Mirabal-García, J.M. Martínez-Huerta, J.G. Cabal Velarde, I.E. Castaneda-Robles, A. Lobo-Guerrero, Analysis of the magnetic properties in hard-magnetic nanofibers composite, J. Appl. Phys. 123 (2018) 105108.

[24] D. Neupane, M. Ghimire, H. Adhikari, A. Lisfi, S.R. Mishra, Synthesis and magnetic study of magnetically hard-soft $SrFe_{12-y}Al_yO_{19}$ – x Wt.% $Ni_{0.5}Zn_{0.5}Fe_2O_4$ nanocomposites, AIP Adv. 7 (2017) 055602.